PHYSICAL REVIEW B **81**, 121407(R) (2010)

Probing charging and localization in the quantum Hall regime by graphene *p–n–p* junctions

Jairo Velasco, Jr., Gang Liu (刘钢), Lei Jing (荆雷), Philip Kratz, Hang Zhang (张航), Wenzhong Bao (包文中), Marc Bockrath, and Chun Ning Lau (劉津寧)*

Department of Physics and Astronomy, University of California, Riverside, California 92521, USA

(Received 7 December 2009; revised manuscript received 25 January 2010; published 9 March 2010)

Using high-quality graphene *pnp* junctions, we observe prominent conductance fluctuations on transitions between quantum Hall (QH) plateaus as the top gate voltage V_{tg} is varied. In the V_{tg}-B plane, the fluctuations form crisscrossing lines that are parallel to those of the adjacent plateaus, with different temperature dependences for the conductance peaks and valleys. These fluctuations arise from Coulomb-induced charging of electron- or hole-doped localized states when the device bulk is delocalized, underscoring the importance of electronic interactions in graphene in the QH regime.

DOI: 10.1103/PhysRevB.81.121407 PACS number(s): 73.43.−f, 73.22.−f, 73.23.−b

Graphene's unique electrical,[1,2] thermal,[3] and mechanical[4,5] properties have made it a topic of intense focus. Electronic interactions in graphene have been predicted to play important roles in its electronic properties because of the enhanced Coulomb repulsion and reduced screening in this strictly two-dimensional (2D) system. In particular, interaction effects are predicted to have profound effects on graphene in the quantum Hall (QH) regime,[6,7] as confirmed by the recent observation of fractional quantum Hall effect in high mobility suspended graphene devices.[8,9] Nevertheless, most of the experimental results in graphene in the integer QH regimes can be satisfactorily interpreted by single-particle pictures,[10,11] and the evidence for interaction effects has remained surprisingly elusive.

In this Rapid Communication we present conductance measurement of high-quality graphene *pnp* junctions[12–17] with suspended top gates in the QH regime. In magnetic fields $B>3$ T, the devices display well-developed conductance plateaus at uniform charge density n, with up to 15 discernible plateaus. Interestingly, we observe reproducible conductance fluctuations between quantum Hall plateaus when the charge density of the top-gated region n_{tg} is modulated. In the n_{tg}-B plane, slopes of these fluctuations are parallel to those of the center of the adjacent plateaus with integer filling factors. We attribute such QH fluctuations to Coulomb-induced charging of localized states in the device,[18–20] which are estimated to be 80–130 nm in diameter. Notably, for the zeroth Landau level (LL), both positive and negative slopes in the n_{tg}-B plane are observed, indicating the evolution of both hole- and electron-doped states. Moreover, with increasing temperature, the conductance of the peaks of the fluctuations remain constant, while those of the valleys increase, in agreement with the behavior of a Coulomb-blockaded quantum dot. Our results reflect the importance of electronic interaction in the QH regime in graphene and demonstrate that electrical transport in *pnp* junctions uniquely reveals both local and global properties of the devices.

The substrate consists of a 300 nm SiO_2 layer grown over degenerately doped silicon, which serves as a global back gate. Graphene sheets are deposited onto the substrate by the standard micromechanical exfoliation method[10,21] and identified by color contrast in an optical microscope and Raman spectroscopy.[22] The electrodes, which consist of 10 nm of Ti and 80 nm of Al, are deposited on graphene using standard electron-beam lithography. A multilevel lithography process[23,24] is used to fabricate a suspended top gate that straddles the center portion of graphene [Figs. 1(a) and 1(b)]. Since no dielectric material directly contacts the single atomic layer, these graphene devices are exceedingly clean.[24] The air gap between the top gate and graphene also allows surface adsorbates, including those directly under the top gate, to be removed via annealing.[25] As a demonstration, we measure the two-terminal conductance G of a graphene device as a function of the applied back gate voltage V_{bg} both before and after annealing in vacuum at 120 °C [Fig. 1(c)]. The $G(V_{bg})$ characteristics is considerably improved upon annealing, with a sharper Dirac point that is closer to zero, indicating the removal of undesirable adsorbates and resist residue.

The graphene devices are measured at 260 mK using standard lock-in techniques. Similar data are observed in five devices. Here, we focus on data from a single device, with a source-drain separation $L=1.4$ μm; the width of the graphene sheet is 1.8 μm at the source and 1.4 μm at the drain electrodes, respectively. The top gate is suspended at a distance $t\sim 100$ nm above the substrate, covering a 400-nm-long segment of the device.

At high magnetic fields, graphene's relativistic band structure gives rise to LLs with energies $E_N=\mathrm{sgn}(N)\sqrt{2e\hbar v_F^2|N|B}$ (Ref. 2); between the LLs, the device conductance is quantized at $4(N+\frac{1}{2})(e^2/h)$. Here, N is an integer denoting the LL index, e is the electron charge, h is Planck's constant, and $v_F\sim 10^6$ m/s is the Fermi velocity of the charges. The upper panel in Fig. 1(d) plots G in units of e^2/h vs V_{bg} at $B=8$ T with the top gate disconnected, and clear plateaus at $\nu=2$, 6, 10, 14, and 18 with almost perfectly quantized conductances are observed, where $\nu=nh/Be$ is the filling factor and n is the electrostatically induced charged density in graphene. The standard "fan diagram" of QH plateaus is shown in the lower panel in Fig. 1(d), for B ranges from 2 to 8 T and V_{bg} ranges from −5 to 50 V. A total of 15 QH plateaus are discernible (although conductance for plateaus for $\nu>20$ is not exactly quantized), and the $2e^2/h$ plateau is quantized at magnetic field as low as 2.5 T. All these features underscore the high quality of the device.

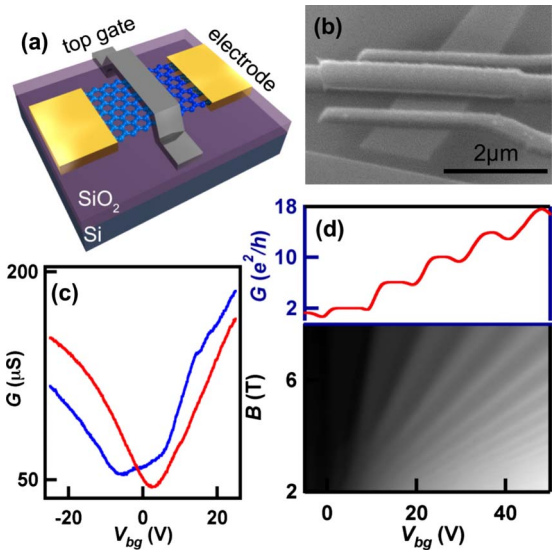

FIG. 1. (Color online) (a) and (b) Schematic and scanning electron microscope image of a device. (c) $G(V_{bg})$ of a device before (left trace) and after (right trace) annealing. (d) Upper panel: $G(V_{bg})$ at $B=8$ T. Lower panel: G (gray scale) vs V_{bg} and B.

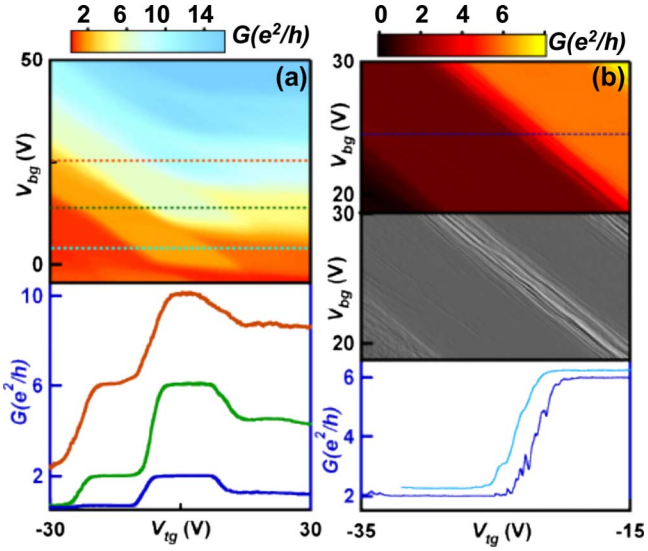

FIG. 2. (Color online) (a) $G(V_{bg},V_{tg})$ at $B=8$ T and $T=260$ mK. The curves in the lower panel are line traces along the dotted lines in the color plot, i.e., from top to bottom, at $\nu_1=2$, 6, and 10, respectively. (b). Upper panel: same as (a) but at high gate voltage resolutions. Middle panel: $dG/dV_{tg}(V_{bg},V_{tg})$ by differentiating data in the upper panel. Lower panel: (lower curve) line trace along the dotted line in the upper panel; (upper curve) same data as the red curve but taken with medium V_{tg} resolution and offset for clarity.

From the fan diagram, the plateaus' centers have slopes in the V_{bg}-B plane given by

$$b_{bg} = \nu e/h\alpha_{bg}, \tag{1}$$

where $\alpha_{bg}=n/V_{bg}$ is the coupling efficiencies for the back and top gates, respectively, and $\nu=4(N+\frac{1}{2})=2,6,10,\ldots$. In Fig. 1(d), for the $N=0$, 1, and 2 plateaus, the slopes are measured to be $b_{bg}=0.74$, 2.0, and 3.4, respectively, yielding $\alpha_{bg}\sim 7.5\times 10^{10}$ cm^{-2} V^{-1}, in good agreement with that estimated from geometric considerations.

By applying voltages to both top and back gates, we modulate the induced charge density in the top-gated and non-top-gated regions, thus creating *pnp* junctions with *in situ* tunability and dopant levels. In the QH regime, the nonuniform charge density gives rise to regions of different filling factors and, for bipolar (i.e., *pnp* or *npn*) junctions, counterpropagating edge states. Consequently, the device conductance exhibits plateaus at fractional values of e^2/h that arise from the mixing of edge states at the interfaces. Assuming full edge state equilibration, the device conductance is given by[13]

$$G = e^2/h|\nu_2| \quad \text{if} \quad \nu_1\nu_2 > 0, \quad |\nu_1| \geq |\nu_2|, \tag{2a}$$

$$G = \frac{e^2}{h}\left(\frac{1}{|\nu_1|} \mp \frac{1}{|\nu_2|} + \frac{1}{|\nu_1|}\right)^{-1} \times \begin{cases} -: \text{if} \quad \nu_1\nu_2 > 0, & |\nu_2| > |\nu_1| \\ +: \text{if} \quad \nu_1\nu_2 L < 0, \end{cases} \tag{2b}$$

where ν_1 and ν_2 are the filling factors in the areas outside and within the top-gated regions, respectively. As shown in Fig. 2(a), a typical QH map $G(V_{bg},V_{tg})$ at $B=8$ T appears as a plaque of adjoined parallelograms with different colors, representing QH plateaus at different combinations of ν_1 and ν_2. The slope of the diagonal lines, which is measured to be ~ 0.8, yields the ratio of the coupling efficiencies between the two gates. This agrees with that estimated from a simple model of parallel plate capacitance, given by $\eta=d/(t\varepsilon_{\mathrm{SiO}})\sim 0.77$, where $d=300$ nm and $\varepsilon_{\mathrm{SiO}}=3.9$ are the thickness and the dielectric constant of the SiO_2 layer. Thus, the top gate efficiency $\alpha_{tg}=n/V_{tg}$ is estimated to be 6×10^{10} cm^{-2} V^{-1}. Three line traces $G(V_{tg})$ at $\nu_1=2$, 6, and 10 are displayed in the lower panel in Fig. 2(a). The measured conductance values of the plateaus are in excellent agreement with that obtained from Eqs. (2). Although similar data have been reported before,[12,13,26,27] we would like to emphasize that this data set demonstrates fully developed and properly quantized plateaus up to the $N=2$ LL in graphene *npn* and *nn'n* junctions, again underscoring the high junction quality.

Interestingly, although the transitions between QH plateaus appear to be smooth in Fig. 2(a), more complicated structures develop upon high-resolution $G(V_{bg},V_{tg})$ scans. Figure 2(b) presents data over a smaller range of that in Fig. 2(a), but taken with 20 times higher gate voltage resolutions at 5 mV/pixel in V_{bg} and 50 mV/pixel in V_{tg}. Instead of smooth steps, the transitions between different QH plateaus now display pronounced fluctuations. A line trace of the transition between $G=2e^2/h$ and $6e^2/h$ plateaus is shown in the lower panel (lower curve). To identify the movement of such fluctuations more clearly, we plot dG/dV_{tg} in the middle panel in Fig. 2(b). Evidently, these fluctuations are observed on all the transitions between different plateaus. Moreover, even though similar conductance fluctuations can be observed in high-resolution $G(V_{bg})$ plots when the device has uniform charge density (i.e., with the top gate disconnected),

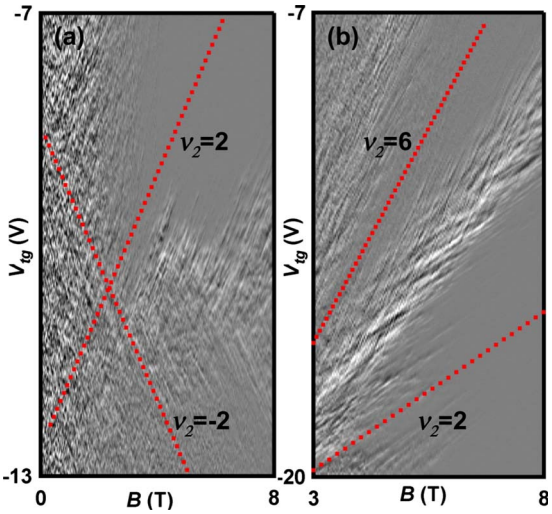

FIG. 3. (Color online) $dG/dV_{tg}(V_{tg},B)$ at (a) $V_{bg,}=2.5$ or $\nu_1 \approx 2$, and (b) $V_{bg,}=14$ or $\nu_1 \approx 6$. The dotted lines indicate the trajectory of the QH plateaus in the locally gated area.

the amplitudes are significantly smaller, indicating the local nature of these fluctuations.

We note that with medium-resolution scans (at 25 mV/pixel in V_{bg}), these fluctuations appear as kinks or small plateaus on the transition, as shown by the upper curve in Fig. 2(b), and may resemble that arising from spin- or valley-resolved LL or even fractional QHE. To elucidate the origin of these fluctuations, we study their evolution with V_{tg} and B at constant V_{bg}. Figure 3(a) plots the differentiated conductance dG/dV_{tg} as a function of V_{tg} and B at $V_{bg}=2.5$ V or, equivalently, at $\nu_1=2$. At $B=8$ T, the conductance changes from $0.67e^2/h$ at $V_{tg}=-13$ V (or $\nu_2 \sim -1.7$) to $2e^2/h$ at $V_{tg}=-7$ V (or $\nu_2 \sim 0.2$). Figure 3(b) plots another data set $dG/dV_{tg}(V_{tg},B)$, taken at $V_{bg}=14$ V or $\nu_1=6$. At $B=8$ T, the conductance increases from $2e^2/h$ at $V_{tg}=-20$ V (or $\nu_2 \sim 0.5$) to $2e^2/h$ at $V_{tg}=-7$ V (or $\nu_2 \sim 4.6$). In both graphs, two pronounced features become evident: "smooth" sections that increase in area with increasing magnetic field, separated by strips of "rough areas" that stay approximately constant in size. In the smooth regions, $dG/dV_{tg}=0$, so they correspond to QH plateaus in the locally gated area; as the energetic spacing between LLs increases with magnetic fields, the width of a given smooth region grows accordingly. The red dotted lines plot the slopes of the plateaus in the V_{tg}-B plane, given by b_{bg}/η, which are calculated using values of b_{bg} measured from Fig. 1(d) and $\eta=0.8$ from Fig. 2(a).

We now focus on the rough areas separating the QH plateaus in Fig. 3. They consist of crisscrossing bright and dark lines, corresponding to extrema values in conductance fluctuations between QH transitions. Noticeably, trajectories of these ridges are parallel to the dotted lines or to the adjacent QH plateaus. For instance, in Fig. 3(b), the rough area separating the $2e^2/h$ and $6e^2/h$ plateaus consists of lines with the same slopes as the $\nu_2=2$ and 6 plateaus; in Fig. 3(a), the lines are parallel to the $\nu_2=-2$ and 2 plateaus, respectively. In the low-B (lower left) corner of Fig. 3(b), several short lines parallel to the $\nu_2=2$ plateau are visible, but abruptly stop as the device conductance become quantized at higher fields.

Such conductance fluctuations between QH transitions have been observed in metal-oxide-semiconductor field-effect transistor (MOSFET) devices,[18] although only with positive slopes. Very recently, conductance fluctuations are also observed in graphene, but at low magnetic field ($B<1$ T) and only near the Dirac point.[28] In the single-particle picture, these fluctuations may arise from resonant tunneling between the edge states on opposite sides of the device through states located in the bulk.[29] However, trajectories of these fluctuations are expected to be parallel to that of half-integer values of filling factors.[18] Thus, we attribute these fluctuations to charging and localization induced by electronic interactions. Assuming a general disorder potential induced by, e.g., impurities on the substrate or graphene, the electron density in graphene develops local valleys and hills. At high magnetic fields, the edge channels in a 2D electron system form compressible and incompressible strips, with contours that generally follow the local potential landscapes. Thus, when an incompressible (insulating) strip completely surrounds a compressible (metallic) region, this effectively creates a quantum dot with quantized charges. The conductance fluctuations then arise from charging of and transport across one or multiple such quantum dots, and these should only depend on the geometry of the dots.[30] Since the filling factor ν within an incompressible strip takes on integer values, which only depends on the ratio n/B, the size of the dot (and hence the fluctuations) should remain constant for the same n/B value, as observed experimentally. We note that, in contrast to MOSFET devices,[18] fluctuations with both positive and negative slopes in the V_{tg}-B plane are observed, indicating the presence of both electron- and hole-doped incompressible strips at the $N=0$ LL, a manifestation of graphene's unique band structure.

Our data shown in Fig. 3(b), i.e., the parallel lines with slopes given by Eq. (1) for $\nu=-2,2,6,\ldots$, bear striking resemblance with that of local inverse electronic compressibility of graphene[19] and GaAs/AlGaAs (Ref. 20) devices using scanning single electron transistors (SETs), albeit with one important difference: in the SET measurements, the line appears on the QH plateaus, at which the bulk of the device consists of incompressible states; in our experiment, the lines appear at the transitions or, equivalently, at the center of the Landau levels, when states in the bulk of the graphene are metallic and delocalized.

More supporting evidence is given by the quasiperiodic nature of some of the conductance fluctuations, with a typical separation in V_{tg} of $\Delta V_{tg} \sim 0.1-0.35$ V. In the Coulomb blockade scenario, this represents the charging of a compressible quantum dot that dominates transport. The addition of one electron requires $\Delta V_{tg}=e/(\varepsilon_0 A/t)$, where ε_0 is the permittivity of vacuum and A is the area of the metallic region. This yields a typical metallic area with a diameter of $\sim 80-135$ nm, consistent with SET (Refs. 19 and 31) and other transport measurements.[28] Moreover, when a LL is almost completely filled, an incompressible strip percolates through the metallic regions, marking the onset of QH conductance plateaus. This corresponds to the short parallel lines that abruptly terminate just before the onset of QH conductance plateaus, as seen in the lower left corner of Fig. 3(b).

Finally, we study the temperature dependence of these

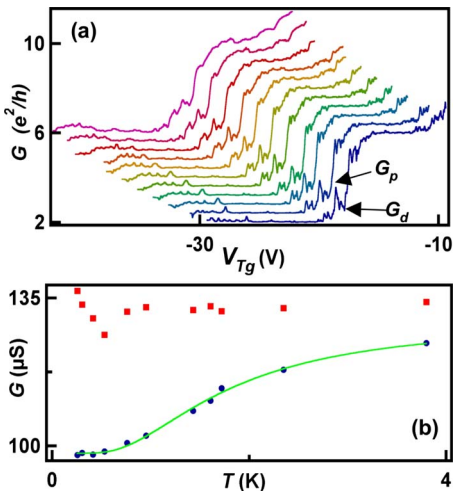

FIG. 4. (Color online) (a) $G(V_{tg})$ for a transition between the $\nu_2=2$ and 6 plateaus. From right to left, $T=0.26$, 0.31, 0.42, 0.53, 0.76, 0.95, 1.43, 1.61, 1.72, 2.35, and 3.8 K. The traces are offset for clarity. (b) T dependence of G_p (red squares) and G_d (blue dots). The green solid line is a fit using Eq. (3).

fluctuations. We focus on the transition between $\nu_2=2$ and 6 plateaus, whereas the non-top-gated regions are kept at $\nu_1=6$. The data are taken at $B=8$ T and ten different temperatures T between 0.26 and 3.8 K [Fig. 4(a)]. In particular, we follow the evolution of the group of fluctuations near the center of the transition, as marked by the arrows in Fig. 4(a). Interestingly, with increasing T, the conductance of the peak of these fluctuations G_p remains approximately constant, while that of the dips G_d increases [Fig. 4(b)]. This is exactly expected for a Coulomb-blockaded classical quantum dot:[30] the dot's maximum conductance is temperature independent, as it is simply determined by the Ohmic addition of the barrier resistances; the minimum conductance of the dot, however, is thermally activated. Thus, our data suggest that a single quantum dot dominates the conductance fluctuations. Modeling the conductance between the QH transitions by that of a single dot in parallel with other metallic paths, we write G_d as[30]

$$G_d(T) = \frac{A/k_BT}{\sinh(\delta/k_BT)} + C, \tag{3}$$

where δ is the energy detuning from the resonant level and k_B is the Boltzmann constant. Using $A=123k_B$, $\delta=4.0k_B$, and $C=98$ μS, we plot the resultant curve as the green line in Fig. 4(b), which is in excellent agreement with the data.

We thank Gil Refael and Shan-Wen Tsai for helpful discussions, and Peng Wei for the assistance with the LABVIEW software. This work was supported in part by NSF CAREER Grant No. DMR/0748910, NSF Grant No. ECCS 0926056, ONR Grant No. N00014-09-1-0724, and UCOP.

*lau@physics.ucr.edu

[1] K. S. Novoselov *et al.*, Science **306**, 666 (2004).
[2] A. H. Castro Neto, F. Guinea, N. M. R. Peres, K. S. Novoselov, and A. K. Geim, Rev. Mod. Phys. **81**, 109 (2009).
[3] A. A. Balandin, S. Ghosh, W. Bao, I. Calizo, D. Teweldebrhan, F. Miao, and C. N. Lau, Nano Lett. **8**, 902 (2008).
[4] C. Lee, X. Wei, J. W. Kysar, and J. Hone, Science **321**, 385 (2008).
[5] W. Z. Bao *et al.*, Nat. Nanotechnol. **4**, 562 (2009).
[6] Y. Zhang, Z. Jiang, J. P. Small, M. S. Purewal, Y. W. Tan, M. Fazlollahi, J. D. Chudow, J. A. Jaszczak, H. L. Stormer, and P. Kim, Phys. Rev. Lett. **96**, 136806 (2006).
[7] K. Nomura and A. H. MacDonald, Phys. Rev. Lett. **96**, 256602 (2006).
[8] X. Du, I. Skachko, F. Duerr, A. Luican, and E. Y. Andrei,Nature (London) **462**, 192 (2009).
[9] K. I. Bolotin, F. Ghahari, M. D. Shulman, H. L. Stormer, and P. Kim, Nature (London) **462**, 196 (2009).
[10] K. S. Novoselov *et al.*, Nature (London) **438**, 197 (2005).
[11] Y. B. Zhang, Y.-W. Tan, H. L. Stormer, and P. Kim, Nature (London) **438**, 201 (2005).
[12] J. R. Williams, L. DiCarlo, and C. M. Marcus, Science **317**, 638 (2007).
[13] B. Özyilmaz, P. Jarillo-Herrero, D. Efetov, D. A. Abanin, L. S. Levitov, and P. Kim, Phys. Rev. Lett. **99**, 166804 (2007).
[14] B. Huard, J. A. Sulpizio, N. Stander, K. Todd, B. Yang, and D. Goldhaber-Gordon, Phys. Rev. Lett. **98**, 236803 (2007).
[15] R. V. Gorbachev *et al.*, Nano Lett. **8**, 1995 (2008).
[16] D. A. Abanin and L. S. Levitov, Science **317**, 641 (2007).
[17] V. V. Cheianov and V. I. Fal'ko, Phys. Rev. B **74**, 041403(R) (2006).
[18] D. H. Cobden, C. H. W. Barnes, and C. J. B. Ford, Phys. Rev. Lett. **82**, 4695 (1999).
[19] J. Martin *et al.*, Nat. Phys. **5**, 669 (2009).
[20] S. Ilani, J. Martin, E. Teitelbaum, J. H. Smet, D. Mahalu, V. Umansky, and A. Yacoby, Nature (London) **427**, 328 (2004).
[21] F. Miao, S. Wijeratne, Y. Zhang, U. C. Coskun, W. Bao, and C. N. Lau, Science **317**, 1530 (2007).
[22] A. C. Ferrari *et al.*, Phys. Rev. Lett. **97**, 187401 (2006).
[23] G. Liu, J. Velasco, Jr., W. Bao, and C. N. Lau, Appl. Phys. Lett. **92**, 203103 (2008).
[24] J. Velasco, G. Liu, W. Bao, and C. N. Lau,New J. Phys. **11**, 095008 (2009).
[25] J. H. Chen, C. Jang, S. Adam, M. S. Fuhrer, E. D. Williams, and M. Ishigami, Nat. Phys. **4**, 377 (2008).
[26] D. K. Ki and H. J. Lee, Phys. Rev. B **79**, 195327 (2009).
[27] T. Lohmann, K. von Klitzing, and J. H. Smet, Nano Lett. **9**, 1973 (2009).
[28] S. Branchaud, A. Kam, P. Zawadzki, F. Peeters, and A. Sachrajda, Phys. Rev. B **81**, 121406 (2010).
[29] J. K. Jain and S. A. Kivelson, Phys. Rev. Lett. **60**, 1542 (1988).
[30] L. P. Kouwenhoven *et al.*, in *Mesoscopic Electron Transport*, edited by L. L. Sohn, L. P. Kouwenhoven, and G. Schon (Kluwer, Springer, 1997).
[31] J. Martin *et al.*, Nat. Phys. **4**, 144 (2008).